Electronic Supplementary Information (ESI†)

Morphology restrained growth of V_2O_5 by the oxidation of V-MXenes as a fast diffusion controlled cathode material for aqueous Zinc ion batteries

Mugilan Narayanasamy,[a] Balakrishnan Kirubasankar,[a,b] Minjie Shi,[a] Shanmuganathan Velayutham,[a] Bei Wang,[a] Subramania Angaiah, [b] and Chao Yan,*[a]

[a]*School of Materials Science and Engineering, Jiangsu University of Science and Technology, Zhenjiang 212003, PR China*

[b]*Electro-Materials Research Laboratory, Centre for Nanoscience and Technology, Pondicherry University, Pondicherry-605 014, India*

**Corresponding Author,*

Prof. Chao Yan E-mail: chaoyan@just.edu.cn

Section S1 Experimental Section

S1.1 Synthesis of V_2CT_x

Initially, the V_2AlC powder (400 mesh, 98.8%) was purchased from 11 technology Co., Ltd, PR China. 0.5 g of V_2AlC was slowly added into 15 mL of 40 wt% hydrofluoric acid (HF) solution at 40 °C under magnetic stirring for 24 h to completely exfoliate the Al layers. Subsequently, the obtained V_2CT_x was washed repeatedly with deionized water until the pH reached ~7. The as-prepared V_2CT_x was soaked in tetramethylammonium hydroxide (TMAOH) for 18 h at room temperature and centrifugated, dried in vacuum at 60 °C for 7 h.

S1.2 Synthesis of V_2O_5@V_2C nanohybrid

V_2O_5@V_2C nanohybrid was prepared by a simple hydrothermal method. 1 g of V_2CT_x powder was dispersed in 80 mL of DI water and stirred for 2 h. This solution is transferred to 100 mL Teflon-lined autoclave heated at various temperatures such as 160 °C, 180 °C and 200 °C for 12 h and denoted as V-160 °C, V-180 °C and V-200 °C, respectively. A light yellowish black precipitate was centrifugated with distilled water several times and dried at 70 °C to collected V_2O_5@V_2C nanohybrid.

S1.3 Fabrication of the Half Cells and ZIB

The working electrodes composed of active materials, acetylene black, and polyvinylidene fluoride (PVDF) binder in a weight ratio of 70:20:10 was intimately mixed in N-methyl-2-pyrrolidone (NMP) to form uniform slurry. Then the casted film (on graphite paper) was kept at 110 °C for 12 h in a vacuum oven to evaporate the solvent. After cooling down to room temperature and cut into circular discs of 15 mm in diameter. The loading mass of the cathode is in the range of 0.6-0.8 mg (average thickness ~4 μm). Zn sheet was used as counter and reference electrode. The ZIB (CR2032) was fabricated using the prepared V_2O_5@V_2C nanohybrid as the positive electrodes and Zn sheet as the negative electrode in

2.5 M $ZnSO_4$ dissolved in deionized water as the electrolyte and glass microfiber filter membrane used as the separator. Galvanostatic charge/discharge measurements of the coin-type ZIB were carried out using a commercial battery test system (LAND model, CT2001A) in the potential range of 0.2 to 1.4 V at room temperature. Cyclic voltammetry tests were done in the potential range between 0.2 and 1.4 V at different scan rates of 0.5, 1 and 2 mV s^{-1}. The electrochemical impedance spectroscopy (EIS) measurements were also carried out in the frequency range of 10^{-2} to 10^{5} Hz with a perturbation amplitude of 5 mV. The CV and EIS were carried out using an electrochemical analysing equipment (CS350, Electrochemical Workstation, Wuhan Corrtest Instruments Corp., Ltd.).

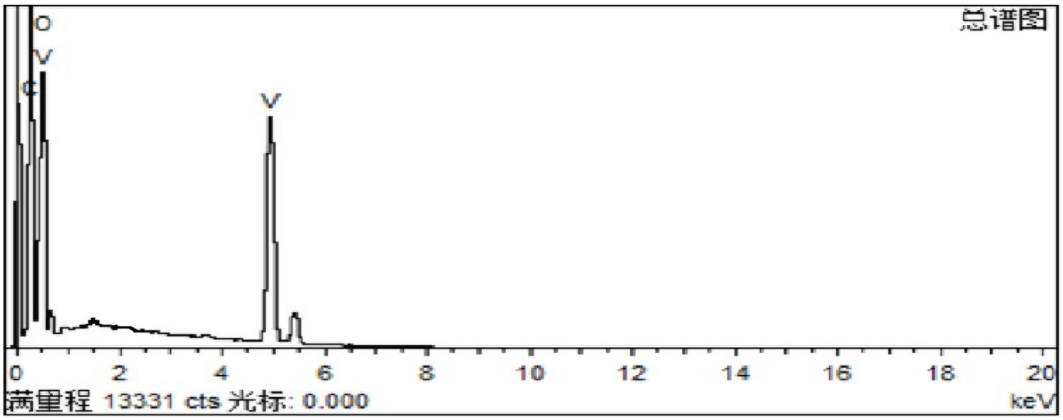

Fig S1. EDS representation V_2O_5@V_2C nanohybrid (V-180°C).

Table S1. Elemental distribution of V, O and C elements of V_2O_5@V_2C nanohybrid at various temperature.

Element	Pure V_2C (wt. %)	160 °C (wt. %)	180 °C (wt. %)	200 °C (wt. %)
V	61.6	52.17	53.38	52.41
C	36.51	31.3	22.15	16.64
O	1.89	16.52	24.47	30.95

The TEM images of V-180 °C are shown in **Fig. S2(a and b)**. Clear V_2O_5 nanorods with an average diameter of ~80 nm and some nanorods are formed internally within the stacked structure, which indicates that V_2O_5 grows not only on the surface of V-MXene but also in-between the stacked layers of V_2C (**Fig. S2a**). **Fig. S2b** presents lattice fringes with interlayer spacings of around 0.34 nm and 0.26 nm which are well-matched with the (110) and (011) planes of V_2O_5. The crystalline V_2C lattice fringe also found at top right with a lattice spacing of 0.29 nm corresponds to the (111) plane of V_2C. These results evidence the growth of V_2O_5 on the surface and interlayers of V-MXene which is well connected with disordered carbons.

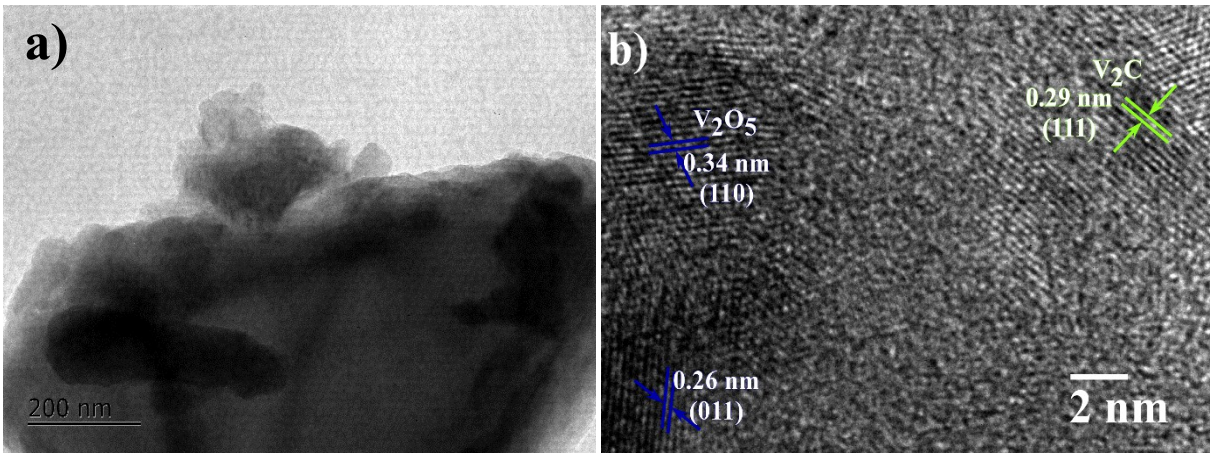

Fig. S2 (a) TEM image of V-180°C and **(b)** HR-TEM image of V-180°C.

In **Fig. 3a** all the CV curves of ZIBs exhibits a similar reduction and oxidation peaks, while V-180 °C shows a maximum current density when compared with V-160 °C and V-200 °C based ZIBs. CV curves of V-160 °C and V-200 °C based electrodes possess lower current due to the morphology retained growth of V_2O_5 on stacked layers of V_2C. In V-160 °C, minimum oxidation occurs and the formation of V_2O_5 is low on V_2C. Hence, the domination of V_2C layered structure minimized the electrochemical kinetic of Zn^{2+} in the host lattice. Whereas in the case of V-200 °C, maximum oxidation occurs, while aggregated thick rods of V_2O_5 formed on V_2C and stacked layers disappear. Hence, the more V_2O_5 can maximize the electrochemical kinetic of Zn^{2+} in the host lattice. However, the surface V_2O_5 is thick and crystallite size is higher, which are detrimental to rate of transfer of electron during the kinetic of Zn^{2+}, tending to possess a lower current density.

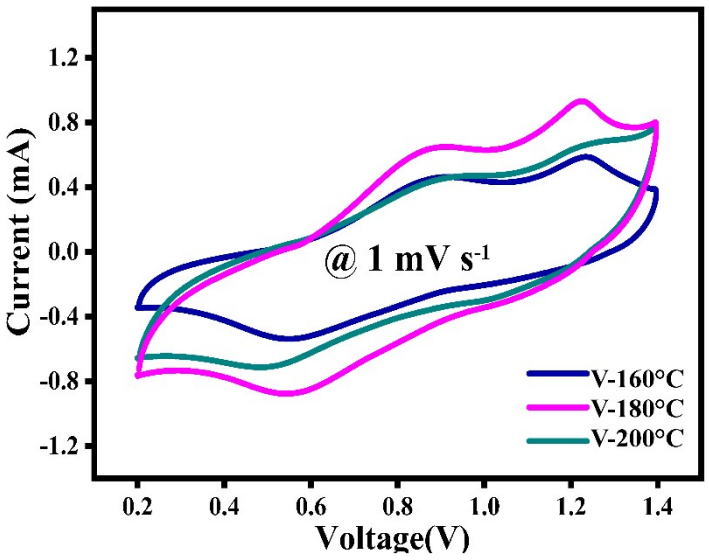

Fig. 3(a) CV curves of V-160°C, V-180°C and V-200°C at 1 mVs^{-1}.

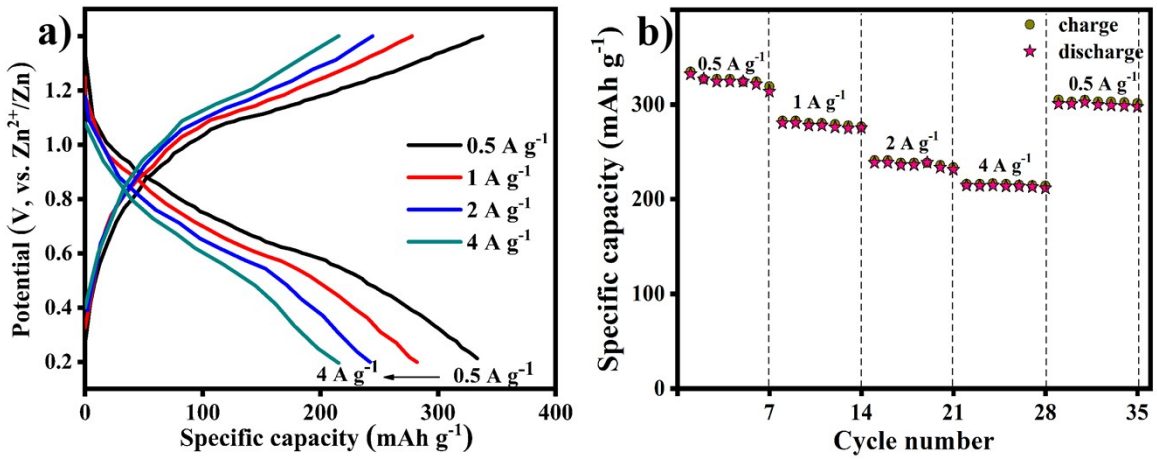

Fig. S3 (a) V-160°C discharge/charge profiles at various current densities and (b) Rate capability of V-160°C.

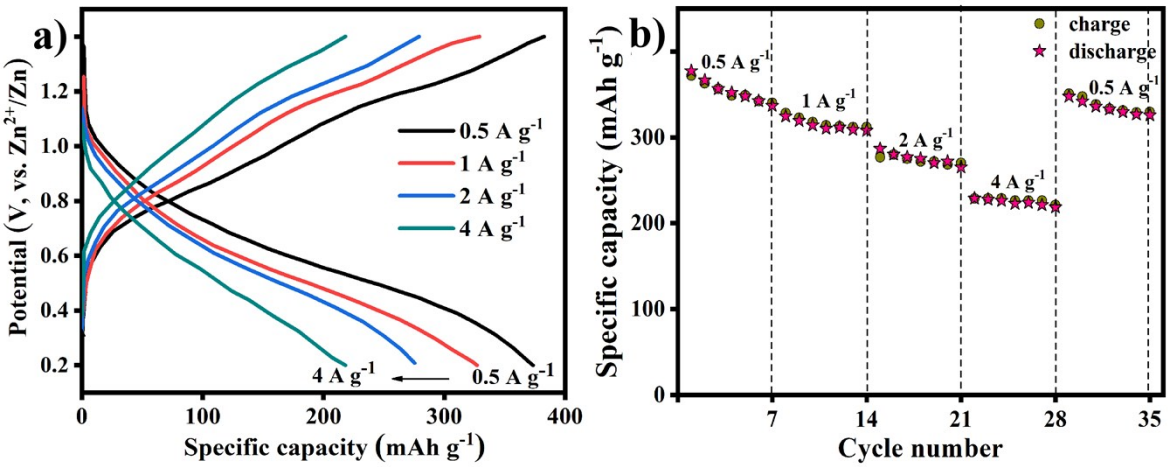

Fig. S4 (a) V-200°C discharge/charge profiles at various current densities and (b) Rate capability of V-200°C.

The cycle stability of V-180 °C ZIB under a low current density of 0.5 A g^{-1} for 100 continuous cycles is shown in **Fig. S5**. A high initial specific capacity of 397 mA h g^{-1} is achieved and well maintains upto the first 10 cycles. A gradual decrease is observed in consecutive cycles and still retain a specific capacity of 336 mA h g^{-1} even after 100 charge-discharge cycles, which indicates better capacity retention of 84.5% with excellent Coulombic efficiency. Mainly, the gradual decrease during cycling process is due to some trapped Zn^{2+} ions into the interior V_2O_5 on stacked layers of V_2C structure, which creates low mass transportation of Zn^{2+} ions and tends to result in capacity fading.

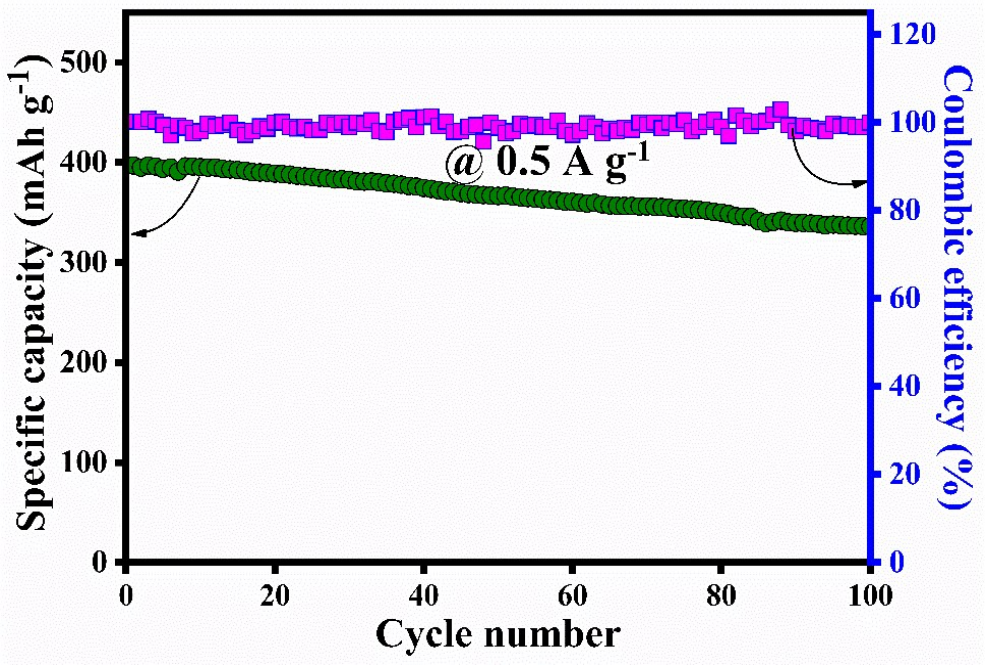

Fig. S5 Cycling performance of V-180°C based ZIB at 0.5 A g^{-1}.

The EIS data is fitted with an equivalent circuit, where R_s denotes bulk resistance due to electrolyte solution, R_{ct} represents charge-transfer resistance indicates the insertion of Zn^{2+} into the V_2O_5@V_2C nanohybrid, CPE account for constant phase elements due to double-layer capacitance arising from the layered structure of V_2C by adsorption/desorption of Zn^{2+} ions, W indicates the Warburg diffusion resistance due to solid-phase diffusion process of Zn^{2+}.

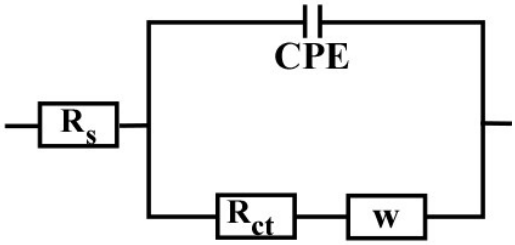

Fig. S6 Equivalent circuit of Nyquist plots.

Fig. S7 shows the increases of (R_{ct}) charge transfer resistance from 47.8 to 77 Ω results from slow mass transfer of Zn^{2+} and the formation of SEI layer during more cycling process.

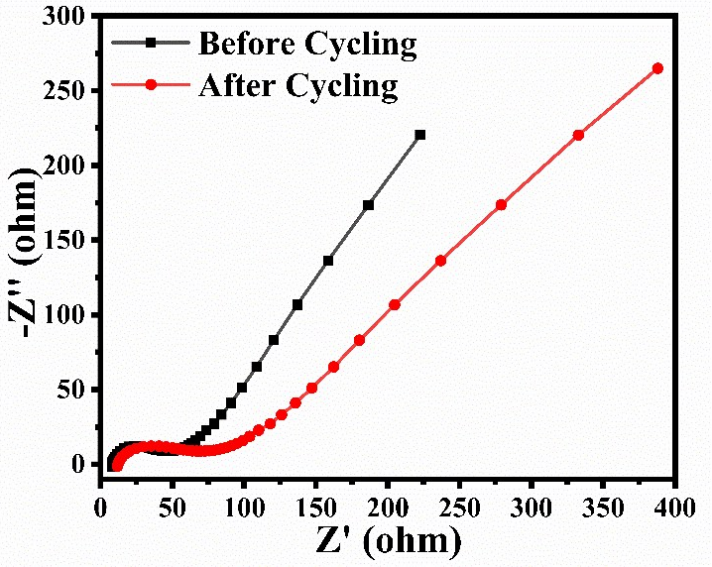

Fig. S7 Nyquist plots of V-180°C based ZIB before and after cycling.

To prove the stability of the V_2O_5@V_2C nanohybrid, we provided the XRD and FESEM analysis of the electrode after cycling (**Fig. S8 & S9**), respectively. XRD analyses before and after cycling (**Fig. S8**) were further carried out to verify the phase stability and structural integrity of V_2O_5@V_2C nanohybrid. It can be clearly observed from the XRD pattern of the electrode after cycling that the characteristic peaks of V_2O_5 and V_2C still exist, while there appears no other impurity peaks compared with the XRD pattern before the cycling test, suggesting that the V_2O_5@V_2C nanohybrid electrode maintains its phase purity and structural integrity after repeated cycling in aqueous ZIBs.

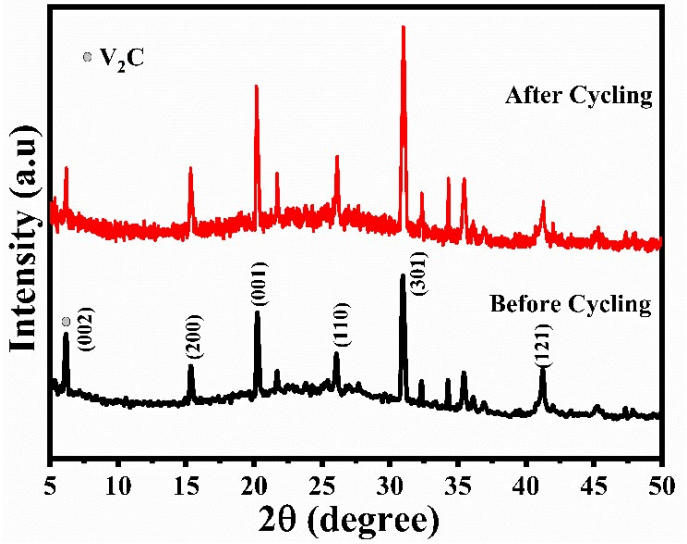

Fig. S8 XRD patterns of V_2O_5@V_2C nanohybrid before and after cycling (V-180°C).

Fig. S9 shows the FESEM image of after cycling. It indicates that there is no obvious structural change or collapse of V_2O_5@V_2C nanohybrid during repeated charging-discharging processes. The effective confinement of V_2O_5 on V_2C stacks can greatly inhibit the aggregation and dissolution of V_2O_5 during the cycling processes, rendering the high stability of the V_2O_5@V_2C nanohybrid on V-180°C electrode for ZIBs.

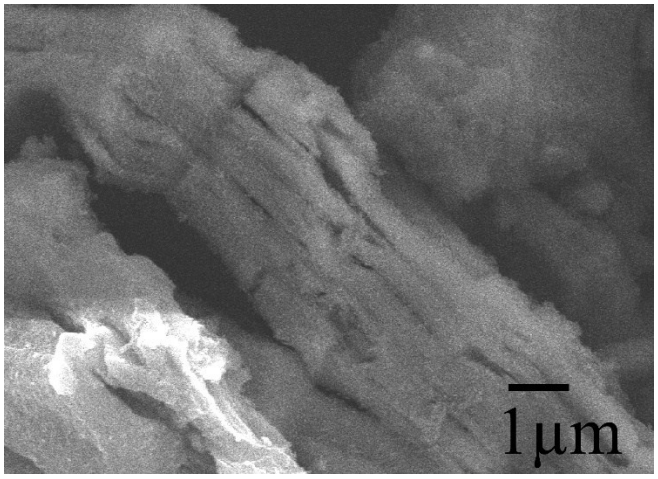

Fig. S9 FESEM image of V_2O_5@V_2C nanohybrid electrode after cycling (V-180°C).

Table S2. Summary of various kinds of V_2O_5 and its composite based cathode material for aqueous ZIBs.

Year of publish	Testing Voltage	Type of V_2O_5	Electrolyte components	Discharge capacity	Capacity Retention
2019[1]	0.2 to 1.6	V_2O_5 hollow spheres	3.5M $ZnSO_4$	280 mA h g^{-1} at 0.2 A g^{-1}	82.5% after 6200 cycles at 10 A g^{-1}
2018[2]	0.4 to 1.4	Commercial V_2O_5	3M $ZnSO_4$	224 mA h g^{-1} at 0.1 A g^{-1}	-
2017[3]	0.2 to 1.6	Porous V_2O_5 microplates	21M LiTFSI and 1M Zn $(CF_3SO_3)_2$	238 mA h g^{-1} at 0.05 A g^{-1}	80% after 2000cycles at 2000 mA g^{-1}
2019[4]	0.2 to 1.6	V_2O_5nanopaper	2M $ZnSO_4$	375 mA h g^{-1} at 0.5 A g^{-1}	76.9% after 500 cycles at 10 A g^{-1}
2019[5]	0.2 to 1.6	Rod-like anhydrous V_2O_5	3 M $Zn(CF_3SO_3)_2$	449.8 mA h g^{-1} at 0.1 A g^{-1}	86.8% after 2000 cycles at 2 A g^{-1}
2019[6]	0.4 to 1.4	Polycrystalline $K_{0.25}$ V_2O_5 nanoparticles	2M $ZnSO_4$	306 mA h g^{-1} at 1 A g^{-1}	83% after 50 cycles at 1 A g^{-1}
2019[7]	0.2 to 1.6	Zn/ V_2O_5	3M $ZnSO_4$(V-3M-Nafion)-seperator	510 mA h g^{-1} at 0.25 A g^{-1}	84% after 1300 cycles at 5 A g^{-1}
2019[8]	0.2 to 1.6	V_2O_5@PEDOT/CC nanosheet	2.5M $Zn(CF_3SO_3)_2$	360 mA h g^{-1} at 0.1 A g^{-1}	97% after 600 cycles at 1 A g^{-1} and 89% after 1000 cycles at 5 A g^{-1}
2019[9]	0.4 to 1.4	K+ intercalated V_2O_5 nanorods	2M $ZnSO_4$	386 mA h g^{-1} at 0.05 A g^{-1}	96% after 1500 cycles at 8000 mA g^{-1}
2019[10]	0.3 to 1.4	Cu-V_2O_5	2M $ZnSO_4$	410 mA h g^{-1} at 0.5 A g^{-1}	-
2019[11]	0.4-1.6	P- V_2O_5	3M $Zn(CF_3SO_3)_2$	320mA h g^{-1} at 0.1 mA g^{-1}	-
2019[12]	0.4-1.6	V_2O_5/CNT	1M $ZnSO_4$	312 mA h g^{-1} at 1 A g^{-1}	81% after 2000 cycles at 1 A g^{-1}
This work	**0.2 to 1.4**	**V_2O_5@V_2C**	**2.5M $ZnSO_4$**	**397 mA h g^{-1} at 0.5 A g^{-1}**	**84.5% after 100 cycles at 0.5A g^{-1} and 87% after 2000 cycles at 4 A g^{-1}**

References

1 H. Qin, L. Chen, L. Wang, X. Chen and Z. Yang, *Electrochim. Acta*, 2019, **306**, 307–316.

2 J. Zhou, L. Shan, Z. Wu, X. Guo, G. Fang and S. Liang, *Chem. Commun.*, 2018, **54**, 4457–4460.

3 P. Hu, M. Yan, T. Zhu, X. Wang, X. Wei, J. Li, L. Zhou, Z. Li, L. Chen and L. Mai, *ACS Appl. Mater. Interfaces*, 2017, **9**, 42717–42722.

4 Y. Li, Z. Huang, P. K. Kalambate, Y. Zhong, Z. Huang, M. Xie, Y. Shen and Y. Huang, *Nano Energy*, 2019, **60**, 752–759.

5 W. Zhou, J. Chen, M. Chen, X. Xu, Q. Tian, J. Xu and C. P. Wong, *RSC Adv.*, 2019, **9**, 30556–30564.

6 S. Li, M. Chen, G. Fang, L. Shan, X. Cao, J. Huang, S. Liang and J. Zhou, *J. Alloys Compd.*, 2019, **801**, 82–89.

7 M. Ghosh, V. Vijayakumar and S. Kurungot, *Energy Technol.*, 2019, **7**, 1–10.

8 D. Xu, H. Wang, F. Li, Z. Guan, R. Wang, B. He, Y. Gong and X. Hu, *Adv. Mater. Interfaces*, 2019, **6**, 1–8.

9 S. Islam, M. H. Alfaruqi, D. Y. Putro, V. Soundharrajan, B. Sambandam, J. Jo, S. Park, S. Lee, V. Mathew and J. Kim, *J. Mater. Chem. A*, 2019, **7**, 20335–20347.

10 Y. Yang, Y. Tang, S. Liang, Z. Wu, G. Fang, X. Cao, C. Wang, T. Lin, A. Pan and J. Zhou, *Nano Energy*, 2019, **61**, 617–625.

11 Y. Ding, Y. Peng, W. Chen, Y. Niu, S. Wu, X. Zhang and L. Hu, *Appl. Surf. Sci.*, 2019, **493**, 368–374.

12 B. Yin, S. Zhang, K. Ke, T. Xiong, Y. Wang, B. K. D. Lim, W. S. V. Lee, Z. Wang and J. Xue, *Nanoscale*, 2019, **11**, 19723–19728.